

Behind the Scenes: Towards Reading Beyond Faces for Sparsity-Aware 4D Affect Recognition

Muzammil Behzad, Nhat Vo, Xiaobai Li, Guoying Zhao

muzammil.behzad@oulu.fi, nhat.vo@oulu.fi, xiaobai.li@oulu.fi, guoying.zhao@oulu.fi
Center for Machine Vision and Signal Analysis (CMVS)
University of Oulu, Finland.

ABSTRACT

In this paper, we present a sparsity-aware deep network for automatic 4D facial expression recognition (FER). Given 4D data, we first propose a novel augmentation method to combat the data limitation problem for deep learning. This is achieved by projecting the input data into RGB and depth map images and then iteratively performing randomized channel concatenation. Encoded in the given 3D landmarks, we also introduce an effective way to capture the facial muscle movements from three orthogonal plans (TOP), the TOP-landmarks over multi-views. Importantly, we then present a sparsity-aware deep network to compute the sparse representations of convolutional features over multi-views. This is not only effective for a higher recognition accuracy but is also computationally convenient. For training, the TOP-landmarks and sparse representations are used to train a long short-term memory (LSTM) network. The refined predictions are achieved when the learned features collaborate over multi-views. Extensive experimental results achieved on the BU-4DFE dataset show the significance of our method over the state-of-the-art methods by reaching a promising accuracy of 99.69% for 4D FER.

CCS CONCEPTS

• **Information systems** → **Specialized information retrieval**; • **Computing methodologies** → **Neural networks**; *Mesh models*; *Point-based models*; **Image processing**.

KEYWORDS

Affect, Augmentation, Deep Learning, 4D Facial Expression Recognition, Landmarks

ACM Reference Format:

Muzammil Behzad, Nhat Vo, Xiaobai Li, Guoying Zhao. 2022. Behind the Scenes: Towards Reading Beyond Faces for Sparsity-Aware 4D Affect Recognition. In *Proceedings of ACM Conference (Conference'20)*. ACM, New York, NY, USA, 8 pages. <https://doi.org/10.1145/nnnnnnn.nnnnnnn>

1 INTRODUCTION

Facial expressions (FEs) are one of the most important, powerful and natural ways to convey and understand human emotions.

Permission to make digital or hard copies of all or part of this work for personal or classroom use is granted without fee provided that copies are not made or distributed for profit or commercial advantage and that copies bear this notice and the full citation on the first page. Copyrights for components of this work owned by others than ACM must be honored. Abstracting with credit is permitted. To copy otherwise, or republish, to post on servers or to redistribute to lists, requires prior specific permission and/or a fee. Request permissions from permissions@acm.org.
Conference'20, October 2020, Seattle, USA

© 2022 Association for Computing Machinery.
ACM ISBN 978-x-xxxx-xxxx-x/YY/MM... \$15.00
<https://doi.org/10.1145/nnnnnnn.nnnnnnn>

Many works have been reported in this regard to automate facial expression analysis due to its tremendous applications in medical diagnosis, social robots, self-driving cars, educational well-being and several other human computer interaction methods. This paved the way for the rise of many facial expression recognition (FER) systems [1] using the recently-trending computer vision technologies with deep learning. Dating back to 1970s, the pioneer study done by Ekman and Friesen [2] discussed the six universal human facial expressions which are happiness, anger, sadness, fear, disgust and surprise.

To recognize such expressions, many machine learning methods have been proposed in the literature which commonly use static or dynamic 2D images. However, such methods face challenging problems of sensitivity towards pose variations, lighting condition changes and occlusions. With the advent of high-speed and high-resolution 3D data acquisition equipment, the research direction is recently steered towards FER systems based on static and dynamic 3D face models. Being more robust towards aforementioned problems, and providing additional geometry information [3], the dynamic 3D data (also known as 4D) conveniently stores the facial deformations when a facial expression is triggered. Importantly, the release of large-size facial expression datasets containing 3D/4D face scans (e.g., the BU-4DFE dataset [4]) has allowed 4D FER by fetching facial deformation patterns both spatially as well as temporally.

1.1 Related Work

To learn from the underlying 3D facial geometry, a number of methods are reported [5], which only rely on the static 3D data, i.e., apex frames. On the other hand, 4D data provides complimentary spatio-temporal patterns allowing deep models to significantly understand and predict the facial expressions. For instance, Sun *et al.* [6] and Yin *et al.* [4] proposed a method based on Hidden Markov Models (HMM) to learn the facial muscle patterns over time. In another attempt, using random forest, Ben Amor *et al.* [7] presented a deformation vector field mainly based on Riemannian analysis to benefit from local facial patterns. Likewise, Sandbach *et al.* [8] proposed free-form deformation as representations of 3D frames and then used HMM and GentleBoost for classification. Moreover, the authors in [9] used support vector machine (SVM) and represented geometrical coordinates and its normal as feature vectors, and as dynamic local binary patterns (LBP) in another work [10]. Similarly, to extract features from polar angles and curvatures, a spatio-temporal LBP-based feature was proposed in [11].

By using the scattering operator [12] on 4D face scans, Yao *et al.* [13] applied multiple kernel learning (MKL) to produce effective feature representations. Similarly, the authors in [14] proposed a

statistical shape model with local and global constraints to recognize FEs. They claimed that local shape index and global face shape can be combined to build a required FER system. For automatic 4D FER via dynamic geometrical image network, an interesting model was proposed by Li *et al.* [15]. They generated geometrical images after the differential quantities were estimated where the final emotion prediction was a function of score-level fusion from different geometrical images. In a similar work, a collaborative cross-domain dynamic image network was proposed by Behzad *et al.*[16] for automatic 4D facial expression recognition. They computed geometrical images and combined their correlated information for a better recognition. Another recent method exploits the sparse coding-based representation of LBP difference [17]. The authors first extracted appearance and geometric features via mesh-local binary pattern difference (mesh-LBPD), and then applied sparse coding to recognize FEs.

1.2 Motivation

Despite many attempts to automate 4D FER, we believe there exist many loopholes that need attention. For example, the data available to train a deep network for 4D FER is very limited. This calls for efficient data augmentation techniques to satisfy the data-hungry nature for deep learning. Moreover, despite the fact that the multi-views of 4D faces jointly capture facial deformations, and that landmarks also encode specific movement patterns, their role is often ignored. Importantly, the need of appropriate facial feature representations is vital in the success of a 4D FER system.

1.3 Contributions

In the light of above discussion, our contributions in this work are 3-fold as follows:

- We present ∞ -augmentation which is a simple yet efficient method to combat 3D/4D data limitation problem.
- We introduce TOP-landmarks over multi-views to extract landmark cues from three orthogonal planes.
- We compute sparse representations from extracted deep features, which outperforms the state-of-the-art performance with reduced computational complexity.

The rest of the paper is organized as follows: our proposed 4D FER method is explained in Section 2. In Section 3, we present and discuss our extensive experimental results to validate the efficiency of the proposed method. Finally, Section 4 concludes the paper.

2 METHOD

In this section, we explain our proposed method for automatic 4D FER. First, we augment our data to extend the dataset size for better deep learning. Second, we extract the facial patterns encoded in landmarks on three orthogonal planes to aid our expression recognition system. We then extract deep features which are then collaboratively learned with landmarks for an accurate expression recognition. To leverage the correlations between ∞ -augmentation, TOP-landmarks and our sparse representations, the proposed sparsity-aware deep learning is explained as follows.

2.1 ∞ -Augmentation

To overcome the limitation of unavailability of large-scale 3D/4D dataset (e.g., only 606 videos in the BU-4DFE [4] dataset), we propose a novel augmentation method. With our simple yet efficient method, the 3D/4D data can be theoretically augmented infinite times, hence the name, ∞ -augmentation. For a given 4D dataset with N examples, we process each 3D point-cloud independently. Therefore, we define

$$I^{4D} = \{I_{nt}^{3D}\}, \forall t = \{1, 2, 3, \dots, T_n\} \text{ and } \forall n = \{1, 2, 3, \dots, N\}, \quad (1)$$

where I^{4D} is the set of 4D face scan examples, and I_{nt}^{3D} denotes n th example and t th temporal frame. Note that (1) $\Rightarrow |I^{4D}| = N$, and $|I_{nt}^{3D}| = T_n$. Consequently for a given 3D point-cloud with M vertices, let us denote its corresponding mesh as

$$\Psi = [\mathbf{v}_1, \dots, \mathbf{v}_M] = [(x_1, y_1, z_1), \dots, (x_M, y_M, z_M)], \quad (2)$$

where $\mathbf{v}_j = [(x_j, y_j, z_j)]$ are the face-centered Cartesian coordinates of the j th vertex. Let us define $f_T : I^{3D} \rightarrow I_T$ to compute the projected RGB texture images, and $f_D : I^{3D} \rightarrow I_D$ to compute the projected depth images from the given mesh via 3D to 2D rendering, where f_T and f_D represent the function mapping from 3D mesh to texture image $I_T \in \mathbb{R}^{K^2}$, and depth image $I_D \in \mathbb{R}^{K^2}$, respectively, where K^2 is the number of pixels. For an image with richer details of the facial deformations, we apply contrast-limited

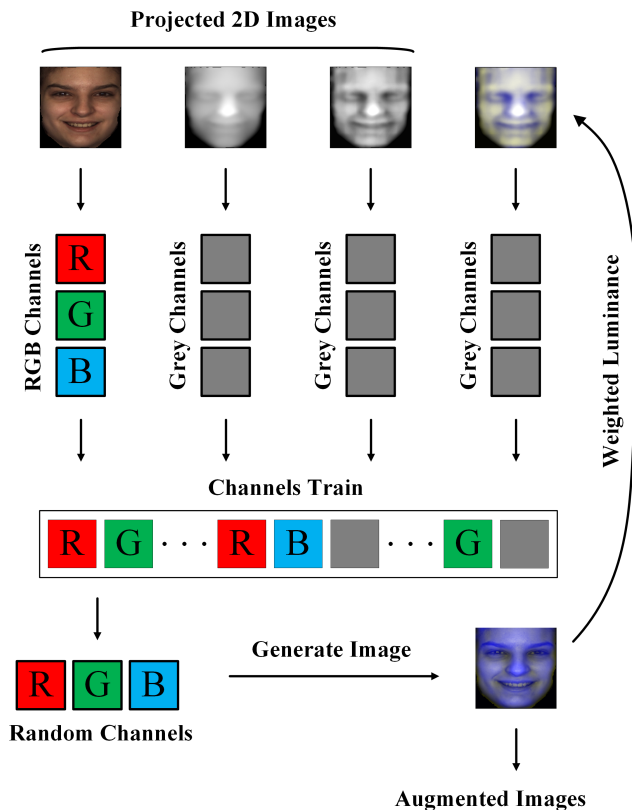


Figure 1: Working flow of the proposed ∞ -augmentation method to generate new images.

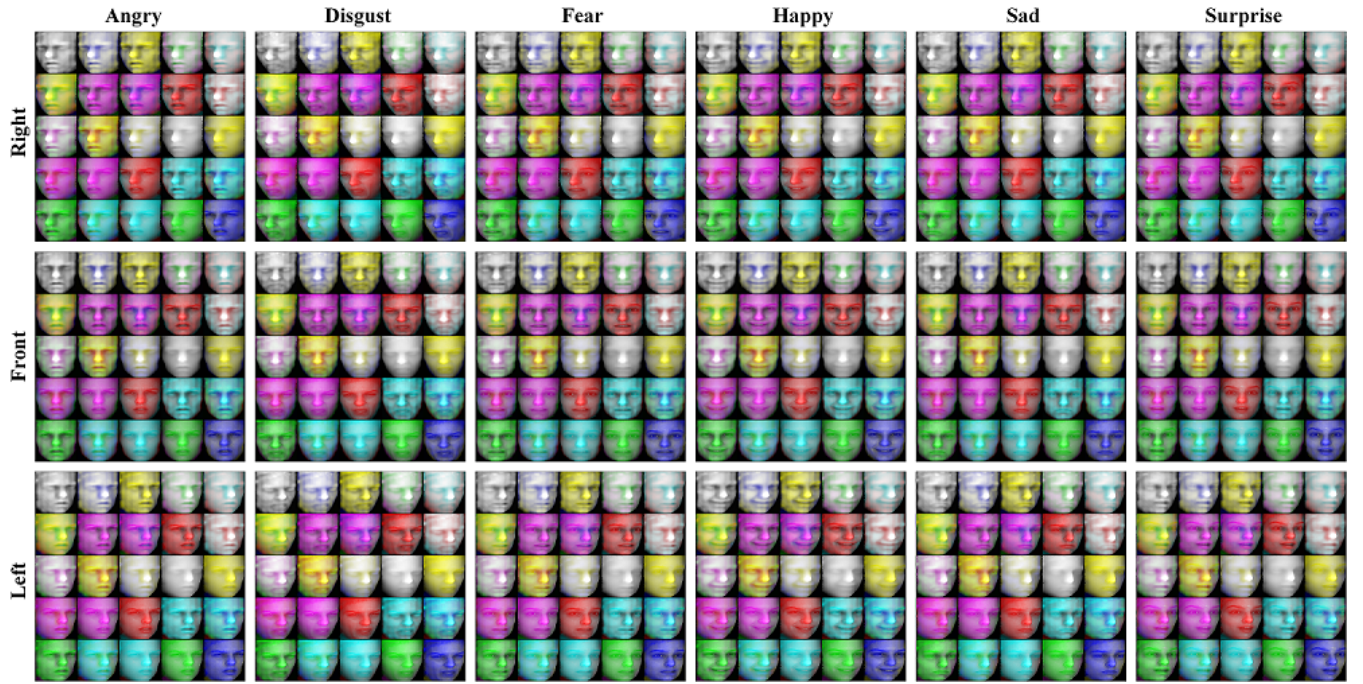


Figure 2: Augmented images generated using our proposed ∞ -augmentation method for each of the six facial expressions. The rows represent the rotation angles at which the expressions are generated, while the columns correspond to the facial expressions. For an expression, we show three different profiles (right, front and left) and twenty five randomly selected samples to validate the effectiveness of our proposed augmentation method. The different colors help in visualizing how the underlying structure of the generated faces is different yet they exhibit similarities which fundamentally helps a deep learning network in identifying meaningful patterns.

adaptive histogram equalization on the depth images to get sharper depth images as $I_{ED} = \eta_s(I_D)$, where $\eta_s(\cdot)$ represents the sharpening operator. Consequently, we get the three projected images as shown in Fig. 1.

Once the projected 2D images are computed, the next step is to separate R/G/B and gray channel(s) of these images and stack them together to form a channels train. Afterwards, randomly selected channels from the channels train are concatenated to generate an augmented image I_G . Inspired by the RGB color model, we then propose to extract the luminance information I_L from the selected channels using a weighted sum as

$$I_L = \alpha_1 I_G^R + \alpha_2 I_G^G + \alpha_3 I_G^B, \quad (3)$$

where α_i is the weight for each of the three R/G/B channels of the generated image I_G . Apart from the standard weights used for extracting luminance in converting a texture RGB image to a gray image ($\alpha_1 = 0.3$, $\alpha_2 = 0.59$, $\alpha_3 = 0.11$), the flexibility in a wide range of weights allows us to perform ∞ -augmentation conveniently. Importantly, by varying the order in which the selected channels are concatenated, and by including the weighted luminance information of an obtained augmented image as an input channel for the next rounds, we iteratively achieve ∞ -augmentation. Note that this process is repeated for each 3D point-cloud or video frame.

In Fig. 2, we show augmented images generated using our proposed ∞ -augmentation method for each of the six universal expressions¹. The rows in this figure represent the rotation angles at which the expressions are generated, while the columns correspond to the facial expressions. For an expression, we show three different profiles (right, front and left) and twenty five randomly selected samples to validate the effectiveness of our proposed augmentation method. The different colors help in visualizing how the underlying structure of the generated faces is different yet they exhibit similarities which fundamentally helps a deep learning network in identifying meaningful patterns. Additionally, apart from the standard weights, the flexibility in choosing weights, the rotation angles and the order of channel concatenation leverages our proposed ∞ -augmentation method and introduces new paradigms in the augmentation community.

2.2 TOP-Landmarks

Inspired by LBP-TOP [18], we propose TOP-landmarks to extract effective landmark cues from three orthogonal planes and then use it in our deep learning network over multi-views (left, front and right). For each of the given multi-views, we first project all the given 3D landmarks over the three XY, XZ and YZ orthogonal planes

¹For a detailed illustration of our proposed ∞ -augmentation method, we suggest the readers to watch the video provided in the supplementary material for a better understanding of how the augmented images/videos appear in real time.

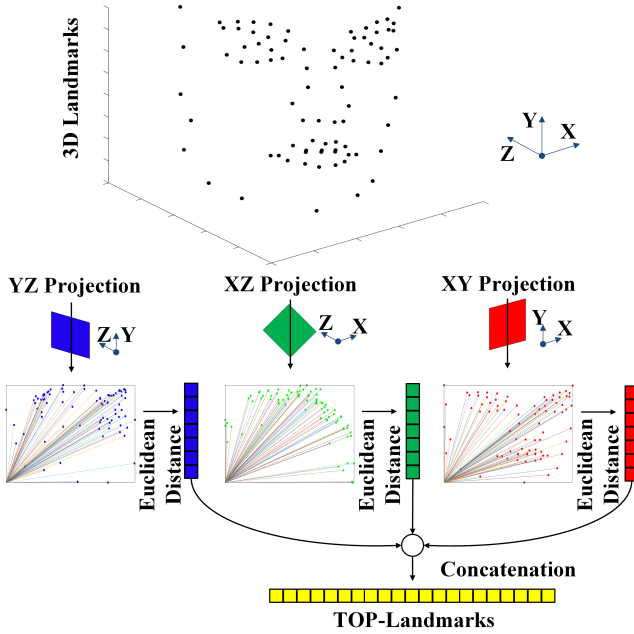


Figure 3: Calculation of TOP-landmarks.

as shown in Fig. 3. Following definitions from (2), this means that for a given set of 3D landmarks with m vertices, the corresponding projections in three orthogonal planes are

$$\begin{aligned}\psi_{XY} &= [\mathbf{v}_1, \dots, \mathbf{v}_m] = [(x_1, y_1), \dots, (x_m, y_m)], \\ \psi_{XZ} &= [\mathbf{v}_1, \dots, \mathbf{v}_m] = [(x_1, z_1), \dots, (x_m, z_m)], \\ \psi_{YZ} &= [\mathbf{v}_1, \dots, \mathbf{v}_m] = [(y_1, z_1), \dots, (y_m, z_m)].\end{aligned}\quad (4)$$

The projected points are then normalized to ensure correspondence across different frames. Next, we compute the Euclidean distance of each landmark point from its origin and store them as distance vectors. Finally, we concatenate the three distance vectors from each orthogonal plane to compute the resultant TOP-landmarks, denoted by Ω , as

$$\Omega = \|\eta(\psi_{XY})\| \frown \|\eta(\psi_{XZ})\| \frown \|\eta(\psi_{YZ})\|, \quad (5)$$

where $\eta(\cdot)$ and \frown denote the normalization and concatenation operators, respectively.

2.3 Sparsity-Aware Deep Learning

Sparsity has recently played a remarkable role in reducing the computation time and boosting classification performance in deep learning [19]. Therefore, we also propose our deep network to be sparsity-aware as shown in Fig. 4. As shown in this figure, once we project the 4D data as RGB texture and depth maps over multi-views, we then augment the data for increasing the training data. Note that instead of using frontal view only, we resort to multi-views and then have a score-level fusion to incorporate the facial muscle movements from the side-views as well. For computational convenience, we use GoogLeNet [20] to extract deep features from the augmented data. From a given 4D face scan, consider an input deep feature vector \mathbf{x}_k with length P , we aim to transform it into

the equivalent sparse representations as

$$\mathbf{x}_k = \mathbf{A}\mathbf{h}_k, \forall k \quad (6)$$

where k is the index for current 3D face, $\mathbf{A} \in \mathbb{R}^{P \times Q}$, $Q \gg P$, is an overcomplete dictionary having wavelet basis. Furthermore, $\mathbf{h}_k \in \mathbb{R}^Q$ is the equivalent sparse representation of the deep feature vector \mathbf{x}_k . For the sparse reconstruction, we let $\hat{\mathbf{h}}_k$ denote an estimate of the sparse vector \mathbf{h}_k obtained via a sparse estimation algorithm [21], and let \mathcal{S}_k represent the set of active indices in the sparse vector, i.e., its support set. For better estimates, each feature vector is processed individually. The estimate of sparse vector \mathbf{h}_k is computed as

$$\hat{\mathbf{h}}_k = \mathbb{E}[\mathbf{h}_k | \mathbf{x}_k] = \sum_{\mathcal{S}_k} p(\mathcal{S}_k | \mathbf{x}_k) \mathbb{E}[\mathbf{h}_k | \mathbf{x}_k, \mathcal{S}_k]. \quad (7)$$

The following explains how the sum, the posterior $p(\mathcal{S}_k | \mathbf{x}_k)$, and the expectation $\mathbb{E}[\mathbf{h}_k | \mathbf{x}_k, \mathcal{S}_k]$ in (7) are evaluated. Given the support \mathcal{S}_k , (6) becomes

$$\mathbf{x}_k = \mathbf{A}_{\mathcal{S}_k} \mathbf{h}_{\mathcal{S}_k}, \quad (8)$$

where $\mathbf{A}_{\mathcal{S}_k}$ is the matrix containing \mathcal{S}_k indexed columns of \mathbf{A} . Likewise, $\mathbf{h}_{\mathcal{S}_k}$ is formed by \mathcal{S}_k indexed entries of \mathbf{h}_k . Since the distribution of \mathbf{h}_k is unknown making $\mathbb{E}[\mathbf{h}_k | \mathbf{x}_k, \mathcal{S}_k]$ very difficult to compute, we use the best linear unbiased estimate (BLUE) as

$$\mathbb{E}[\mathbf{h}_k | \mathbf{x}_k, \mathcal{S}_k] \leftarrow (\mathbf{A}_{\mathcal{S}_k}^H \mathbf{A}_{\mathcal{S}_k})^{-1} \mathbf{A}_{\mathcal{S}_k}^H \mathbf{x}_k, \quad (9)$$

where $(\cdot)^H$ defines the Hermitian conjugate operator. Using Bayes rule, we can write the posterior as

$$p(\mathcal{S}_k | \mathbf{x}_k) = \frac{p(\mathbf{x}_k | \mathcal{S}_k) p(\mathcal{S}_k)}{p(\mathbf{x}_k)}. \quad (10)$$

We can ignore $p(\mathbf{x}_k)$ in (10) as it's a common factor to all posterior probabilities. Since entries of \mathbf{h}_k are activated with Bernoulli distribution having p as success probability, then

$$p(\mathcal{S}_k) = p^{|\mathcal{S}_k|} (1-p)^{Q-|\mathcal{S}_k|}. \quad (11)$$

For $p(\mathbf{x}_k | \mathcal{S}_k)$, if $\mathbf{h}_{\mathcal{S}_k}$ is Gaussian, then $p(\mathbf{x}_k | \mathcal{S}_k)$ would also be Gaussian which is easy to compute. On the contrary, evaluating $p(\mathbf{x}_k | \mathcal{S}_k)$ is difficult for unknown or non-Gaussian $\mathbf{h}_{\mathcal{S}_k}$ distribution. To tackle this, it can be noted that \mathbf{x}_k is formed by a vector in the subspace that is spanned by $\mathbf{A}_{\mathcal{S}_k}$ columns. By projecting \mathbf{x}_k on orthogonal complement space of $\mathbf{A}_{\mathcal{S}_k}$, the distribution can be computed. This is achieved using the projection matrix

$$\mathbf{Z}_{\mathcal{S}_k}^\perp = \mathbf{I} - \mathbf{Z}_{\mathcal{S}_k} = \mathbf{I} - \mathbf{A}_{\mathcal{S}_k} (\mathbf{A}_{\mathcal{S}_k}^H \mathbf{A}_{\mathcal{S}_k})^{-1} \mathbf{A}_{\mathcal{S}_k}^H. \quad (12)$$

Dropping some exponential terms, and simplifying gives us

$$p(\mathbf{x}_k | \mathcal{S}_k) \simeq \exp(-\|\mathbf{Z}_{\mathcal{S}_k}^\perp \mathbf{x}_k\|^2). \quad (13)$$

In this way, we can evaluate the sum in (7) and the sparse representations are computed conveniently as depicted in Fig. 4. This is not only useful for accurate FER due to effective sparse representations, but is also computationally convenient by resizing deep features to fewer samples. For experimental convenience, we use sparse features with thirty samples. Note that our pre-determined dictionary contains wavelet basis which are suitable for the deep features as also validated by the results in the next section.

Finally, we create a long short-term memory (LSTM) network with a sequence input layer, Bi-LSTM layer with 2000 hidden units,

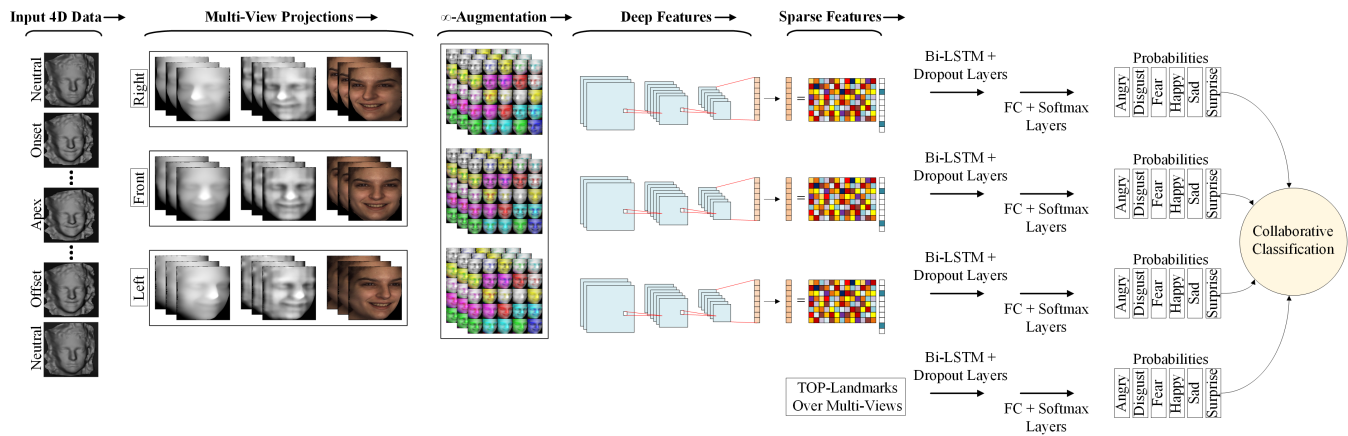


Figure 4: Overview of the proposed sparsity-aware deep learning for 4D affect recognition.

50% dropout layer followed by fully connected (FC), Softmax and classification layer. Consequently, we use the extracted sequences of TOP-landmark and sparse features, all over multi-views, to first train the LSTM network. Afterwards, score-level fusion is performed to collaboratively recognize expressions.

3 EXPERIMENTAL RESULTS

3.1 Dataset and Experimental Settings

To validate the efficiency of our proposed method, we use the BU-4DFE [4] dataset. This dataset contains video clips of 58 females and 43 males (in total 101 subjects) having all six human facial expressions. Each clip has a frame rate of 25 frames per second (fps) lasting approximately 3 to 4 seconds. For experimental settings, we use a 10-fold subject-independent cross-validation (10-CV). Instead of using key-frames [13] or employing sliding windows [8], we use entire 3D sequences. For extracting deep features, we use the pre-trained GoogLeNet [20]. However, we also show our results on other pre-trained models. All of our experiments are carried out on a GP100GL GPU (Tesla P100-PCIE), and the training time takes approximately 3 days. Additionally, unless otherwise stated, three multi-views (right, front and left) and twenty five randomly selected augmented samples are used for all the experiments.

3.2 Effect of ∞ -Augmentation

We evaluate our proposed ∞ -augmentation method over different samples to prove its effectiveness towards deep networks. The accuracies of recognizing facial expressions in the BU-4DFE dataset are compared when different number of samples are generated while augmenting the data. We used random weights for each of the three channels in weighted luminance since the choice of weights is very flexible from 0 to 1. Importantly, to show the effectiveness of our augmentation method, we only do recognition over multi-views, and skip using TOP-landmarks or sparse representations. As shown in Table 1, the results indicate an accuracy jump of 3.52% when augmentation with $5\times$ samples is used. This is related to the effective augmentation strategy where the underlying facial patterns are captured and restored to exhibit similar fundamental

patterns that could help a deep network learn efficiently. This is worth mentioning again that we use a 10-fold subject-independent cross-validation to validate our experiments. This makes our augmentation method robust to over-fitting and makes it capable of performing effectively better in generalized experimental settings. Note that we have used a maximum of $25\times$ augmented samples for convenience. More samples can be chosen at the cost of increased training time.

3.3 Importance of Sparse Representations and TOP-Landmarks

To highlight the importance of sparse representations and TOP-landmarks, we show the confusion matrices of our experiments in Fig. 5. As shown in Fig. 5a, when we use the dense representations only, an accuracy of 93.70% is achieved. In comparison, the upshot of using sparse representations instead of dense representations is an increased accuracy of 94.52%, as shown in Fig. 5b. An intuitively added benefit of the sparsity-aware learning is also the smaller computation time needed to process fewer samples of the sparse representations. A similar trend can be seen while using the TOP-landmarks. For instance, as shown in Fig. 5c, a promising accuracy of 98.78% is achieved when a joint recognition is performed with the help of effective cues computed via TOP-landmarks. It can be analyzed from this figure that despite stronger similarities between angry, disgust and fear expressions, the results indicate that our method accurately predicts the expressions validating its

Table 1: Evaluation of the proposed ∞ -Augmentation method on the BU-4DFE dataset for 4D facial expression recognition (FER).

Augmentation Size	FER Accuracy (%)
No Augmentation	88.45
Augmentation with $5\times$ samples	91.97
Augmentation with $15\times$ samples	93.05
Augmentation with $25\times$ samples	93.70

Angry	247 15.1%	7 0.4%	3 0.2%	0 0.0%	4 0.2%	0 0.0%	94.6% 5.4%
Disgust	9 0.6%	253 15.5%	7 0.4%	2 0.1%	1 0.1%	1 0.1%	92.7% 7.3%
Fear	5 0.3%	19 1.2%	254 15.5%	6 0.4%	5 0.3%	1 0.1%	87.6% 12.4%
Happy	1 0.1%	2 0.1%	11 0.7%	266 16.3%	0 0.0%	0 0.0%	95.0% 5.0%
Sad	7 0.4%	0 0.0%	2 0.1%	0 0.0%	261 16.0%	0 0.0%	96.7% 3.3%
Surprise	0 0.0%	4 0.2%	6 0.4%	0 0.0%	0 0.0%	252 15.4%	96.2% 3.8%
	91.8% 8.2%	88.8% 11.2%	89.8% 10.2%	97.1% 2.9%	96.3% 3.7%	99.2% 0.8%	93.7% 6.3%
	Angry	Disgust	Fear	Happy	Sad	Surprise	

(a) Dense

Angry	266 16.3%	0 0.0%	2 0.1%	0 0.0%	5 0.3%	0 0.0%	97.4% 2.6%
Disgust	3 0.2%	248 15.2%	9 0.6%	8 0.5%	3 0.2%	2 0.1%	90.8% 9.2%
Fear	0 0.0%	3 0.2%	245 15.0%	5 0.3%	0 0.0%	20 1.2%	89.7% 10.3%
Happy	0 0.0%	0 0.0%	0 0.0%	267 16.3%	0 0.0%	6 0.4%	97.8% 2.2%
Sad	14 0.9%	0 0.0%	8 0.5%	0 0.0%	250 15.3%	0 0.0%	91.9% 8.1%
Surprise	0 0.0%	0 0.0%	2 0.1%	0 0.0%	0 0.0%	270 16.5%	99.3% 0.7%
	94.0% 6.0%	98.8% 1.2%	92.1% 7.9%	95.4% 4.6%	96.9% 3.1%	90.6% 9.4%	94.5% 5.5%
	Angry	Disgust	Fear	Happy	Sad	Surprise	

(b) Sparse

Angry	271 16.6%	0 0.0%	0 0.0%	0 0.0%	2 0.1%	0 0.0%	99.3% 0.7%
Disgust	6 0.4%	262 16.0%	3 0.2%	0 0.0%	0 0.0%	2 0.1%	96.0% 4.0%
Fear	0 0.0%	0 0.0%	270 16.5%	0 0.0%	0 0.0%	3 0.2%	98.9% 1.1%
Happy	0 0.0%	1 0.1%	0 0.0%	272 16.6%	0 0.0%	0 0.0%	99.6% 0.4%
Sad	3 0.2%	0 0.0%	0 0.0%	0 0.0%	269 16.4%	0 0.0%	98.9% 1.1%
Surprise	0 0.0%	0 0.0%	0 0.0%	0 0.0%	0 0.0%	272 16.6%	100% 0.0%
	96.8% 3.2%	99.6% 0.4%	98.9% 1.1%	100% 0.0%	99.3% 0.7%	98.2% 1.8%	98.8% 1.2%
	Angry	Disgust	Fear	Happy	Sad	Surprise	

(c) Dense + TOP-L

Angry	273 16.7%	0 0.0%	0 0.0%	0 0.0%	0 0.0%	0 0.0%	100% 0.0%
Disgust	0 0.0%	273 16.7%	0 0.0%	0 0.0%	0 0.0%	0 0.0%	100% 0.0%
Fear	0 0.0%	0 0.0%	271 16.6%	0 0.0%	2 0.1%	0 0.0%	99.3% 0.7%
Happy	0 0.0%	0 0.0%	0 0.0%	273 16.7%	0 0.0%	0 0.0%	100% 0.0%
Sad	0 0.0%	0 0.0%	0 0.0%	0 0.0%	272 16.6%	0 0.0%	100% 0.0%
Surprise	0 0.0%	0 0.0%	3 0.2%	0 0.0%	0 0.0%	269 16.4%	98.9% 1.1%
	100% 0.0%	100% 0.0%	98.9% 1.1%	100% 0.0%	99.3% 0.7%	100% 0.0%	99.7% 0.3%
	Angry	Disgust	Fear	Happy	Sad	Surprise	

(d) Sparse + TOP-L

Figure 5: Comparison of confusion matrices over multi-views for 4D facial expression recognition. [TOP-L = TOP-landmarks]

effectiveness. Finally, as shown in Fig. 5d, a much higher accuracy of 99.6% is achieved when employing sparsity-aware deep learning and TOP-landmarks over multi-views.

3.4 Role of Multi-Views

The results depicted in Fig. 6 compare the contribution and effect of each of the multi-views. These results dictate that our method performs better when all the views are taken into account. For

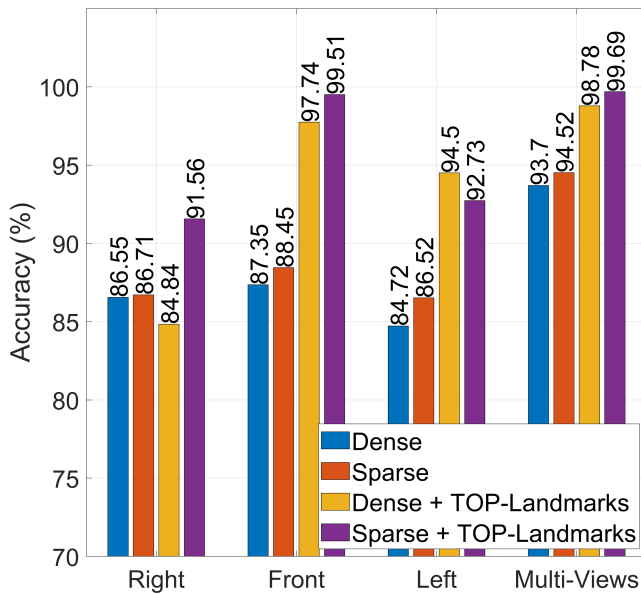


Figure 6: Accuracy (%) comparison over multi-views for 4D facial expression recognition on the BU-4DFE dataset.

example, when we use only the dense representations over multi-views in our model, a promising accuracy of 93.70% is still achieved which shows the effectiveness of the multi-views. Importantly, although the frontal view is more effective in comparison with left and right views, more effective results are achieved when a joint recognition is performed with the help of all these multi-views. More importantly, as discussed previously, a higher accuracy is achieved when both TOP-landmarks and sparse representations are utilized.

3.5 Comparison with the State-of-the-Art Methods

In Table 2, we compare the accuracy of our method with several state-of-the-art methods [3, 6–10, 13, 15, 16, 22, 23] on the BU-4DFE dataset. As illustrated, our method outperforms the existing methods in terms of correct expression recognition. This is mainly due to the extensively collaborative scheme of our method for an accurate expression recognition where the prediction scores are refined from its collaborators. Importantly, we show the effect of using dense vs. sparse representations and also how the TOP-landmarks assist in achieving substantial improvement. As shown, the sparse representations not only intuitively reduce the computational burden but also lead to a more accurate system by less over-fitting and better generalization, hence, raising the accuracy from 93.70% to 98.78%. By using TOP-landmarks, our method further reaches a promising accuracy of 99.69%.

Table 2: Accuracy (%) comparison of 4D facial expression recognition with the state-of-the-art methods on the BU-4DFE dataset. [TOP-L = TOP-landmarks]

Method	Experimental Settings	Accuracy (%)
Sandbach <i>et al.</i> [8]	6-CV, Sliding window	64.60
Fang <i>et al.</i> [10]	10-CV, Full sequence	75.82
Xue <i>et al.</i> [22]	10-CV, Full sequence	78.80
Sun <i>et al.</i> [6]	10-CV, -	83.70
Zhen <i>et al.</i> [3]	10-CV, Full sequence	87.06
Yao <i>et al.</i> [13]	10-CV, Key-frame	87.61
Fang <i>et al.</i> [9]	10-CV, -	91.00
Li <i>et al.</i> [15]	10-CV, Full sequence	92.22
Ben Amor <i>et al.</i> [7]	10-CV, Full sequence	93.21
Zhen <i>et al.</i> [23]	10-CV, Full sequence	94.18
Bejaoui <i>et al.</i> [17]	10-CV, Full sequence	94.20
Zhen <i>et al.</i> [23]	10-CV, Key-frame	95.13
Behzad <i>et al.</i> [16]	10-CV, Full sequence	96.50
Ours (Dense)	10-CV, Full sequence	93.70
Ours (Sparse)	10-CV, Full sequence	94.52
Ours (Dense+TOP-L)	10-CV, Full sequence	98.78
Ours (Sparse+TOP-L)	10-CV, Full sequence	99.69

3.6 Comparison with Other Pre-Trained Models

Finally in Table 3, we compare the results achieved by extracting deep features from other pre-trained models to validate the effectiveness of our method. Specifically, we use AlexNet [24], VGG16 [25], VGG19 [25], Inception-v3 [26], ResNet18 [27], ResNet50 [27] and ResNet101 [27]. The table gives an overall impression that TOP-landmarks significantly improve the recognition accuracy. It also shows a similar trend, as seen in Table 2, that sparse features lead to a better system performance. The superior performance of GoogLeNet is due to several very small convolutions in order to drastically reduce the number of parameters.

Table 3: Accuracy (%) comparison of 4D facial expression recognition on the BU-4DFE dataset by using other pre-trained deep models.

Pre-trained Model	Dense	Dense+TOP-L	Sparse+TOP-L
AlexNet [24]	67.18	82.98	88.55
Inception-v3 [26]	80.01	82.91	89.35
VGG16 [25]	71.45	85.12	89.97
ResNet18 [27]	76.34	87.56	91.60
ResNet101 [27]	76.65	87.71	91.70
ResNet50 [27]	83.74	91.06	93.93
VGG19 [25]	84.54	91.66	94.33
GoogLeNet [20]	93.70	98.78	99.69

4 CONCLUSIONS

We proposed sparsity-aware deep learning to automate 4D FER. We first combated the problem of data limitation for deep learning by introducing ∞ -augmentation. This method uses the projected RGB and depth map images, and then proceed to randomly concatenate them in channels over an iterative process. Second, we explained the idea of TOP-landmarks to capture the encoded facial deformations stored in the 3D landmarks. TOP-landmarks store the facial features from three orthogonal planes by using a distance-based approach. Importantly, we presented our sparsity-aware deep network where the convolutional deep features are used to compute deep sparse features which are then used to train an LSTM network and recognize expressions collaboratively with TOP-landmarks. With a promising accuracy of 99.69%, our method outperformed the existing state-of-the-art 4D FER methods in terms of expression recognition accuracy.

5 ACKNOWLEDGMENTS

This work was supported by Infotech Oulu, the National Natural Science Foundation of China (No. 61772419), Tekes Fidipro Program (No. 1849/31/2015), Business Finland Project (No. 3116/31/2017), and Academy of Finland. As well, the authors wish to acknowledge CSC ÅÅ IT Center for Science, Finland, for computational resources.

REFERENCES

- [1] Shan Li and Weihong Deng. Deep facial expression recognition: A survey. *IEEE Transactions on Affective Computing*, 2020.
- [2] Paul Ekman and Wallace V Friesen. Constants across cultures in the face and emotion. *Journal of personality and social psychology*, 17(2):124, 1971.
- [3] Qingkai Zhen, Di Huang, Yunhong Wang, and Liming Chen. Muscular movement model-based automatic 3d/4d facial expression recognition. *IEEE Transactions on Multimedia*, 18(7):1438–1450, 2016.
- [4] Xing Zhang, Lijun Yin, Jeffrey F Cohn, Shaun Canavan, Michael Reale, Andy Horowitz, and Peng Liu. A high-resolution spontaneous 3d dynamic facial expression database. In *IEEE International Conference and Workshops on Automatic Face and Gesture Recognition*, pages 1–6. IEEE, 2013.
- [5] Huibin Li, Liming Chen, Di Huang, Yunhong Wang, and Jean-Marie Morvan. 3d facial expression recognition via multiple kernel learning of multi-scale local normal patterns. In *Proceedings of the 21st International Conference on Pattern Recognition*, pages 2577–2580. IEEE, 2012.
- [6] Yi Sun, Xiaochen Chen, Matthew Rosato, and Lijun Yin. Tracking vertex flow and model adaptation for three-dimensional spatiotemporal face analysis. *IEEE Transactions on Systems, Man, and Cybernetics-Part A: Systems and Humans*, 40(3):461–474, 2010.
- [7] Boulbaba Ben Amor, Hassen Drira, Stefano Berretti, Mohamed Daoudi, and Anuj Srivastava. 4-d facial expression recognition by learning geometric deformations. *IEEE transactions on cybernetics*, 44(12):2443–2457, 2014.
- [8] Georgia Sandbach, Stefanos Zafeiriou, Maja Pantic, and Daniel Rueckert. Recognition of 3d facial expression dynamics. *Image and Vision Computing*, 30(10):762–773, 2012.
- [9] Tianhong Fang, Xi Zhao, Omar Ocegueda, Shishir K Shah, and Ioannis A Kakadiaris. 3d/4d facial expression analysis: An advanced annotated face model approach. *Image and vision Computing*, 30(10):738–749, 2012.
- [10] Tianhong Fang, Xi Zhao, Shishir K Shah, and Ioannis A Kakadiaris. 4d facial expression recognition. In *IEEE International Conference on Computer Vision Workshops*, pages 1594–1601. IEEE, 2011.
- [11] Michael Reale, Xing Zhang, and Lijun Yin. Nebula feature: A space-time feature for posed and spontaneous 4d facial behavior analysis. In *IEEE International Conference and Workshops on Automatic Face and Gesture Recognition*, pages 1–8. IEEE, 2013.
- [12] Joan Bruna and Stéphane Mallat. Invariant scattering convolution networks. *IEEE transactions on pattern analysis and machine intelligence*, 35(8):1872–1886, 2013.
- [13] Yongqiang Yao, Di Huang, Xudong Yang, Yunhong Wang, and Liming Chen. Texture and geometry scattering representation-based facial expression recognition in 2d+3d videos. *ACM Transactions on Multimedia Computing, Communications, and Applications*, 14(1s):1–23, 2018.
- [14] Diego Fabiano and Shaun Canavan. Spontaneous and non-spontaneous 3d facial expression recognition using a statistical model with global and local constraints. In *IEEE International Conference on Image Processing*, pages 3089–3093. IEEE, 2018.
- [15] Weijian Li, Di Huang, Huibin Li, and Yunhong Wang. Automatic 4d facial expression recognition using dynamic geometrical image network. In *IEEE International Conference on Automatic Face & Gesture Recognition*, pages 24–30. IEEE, 2018.
- [16] Muzammil Behzad, Nhat Vo, Xiaobai Li, and Guoying Zhao. Automatic 4d facial expression recognition via collaborative cross-domain dynamic image network. In *British Machine Vision Conference*, 2019.
- [17] Hela Bejaoui, Haythem Ghazouani, and Walid Barhoumi. Sparse coding-based representation of lbp difference for 3d/4d facial expression recognition. *Multimedia Tools and Applications*, 78(16):22773–22796, 2019.
- [18] Guoying Zhao and Matti Pietikainen. Dynamic texture recognition using local binary patterns with an application to facial expressions. *IEEE transactions on pattern analysis and machine intelligence*, 29(6):915–928, 2007.
- [19] Baoyuan Liu, Min Wang, Hassan Foroosh, Marshall Tappen, and Marianna Pensky. Sparse convolutional neural networks. In *Proceedings of the IEEE conference on computer vision and pattern recognition*, pages 806–814, 2015.
- [20] Christian Szegedy, Wei Liu, Yangqing Jia, Pierre Sermanet, Scott Reed, Dragomir Anguelov, Dumitru Erhan, Vincent Vanhoucke, and Andrew Rabinovich. Going deeper with convolutions. In *Proceedings of the IEEE conference on computer vision and pattern recognition*, pages 1–9, 2015.
- [21] Thomas Blumensath and Mike E Davies. Iterative hard thresholding for compressed sensing. *Applied and computational harmonic analysis*, 27(3):265–274, 2009.
- [22] Mingliang Xue, Ajmal Mian, Wanquan Liu, and Ling Li. Automatic 4d facial expression recognition using dct features. In *2015 IEEE Winter Conference on Applications of Computer Vision*, pages 199–206. IEEE, 2015.
- [23] Qingkai Zhen, Di Huang, Hassen Drira, Boulbaba Ben Amor, Yunhong Wang, and Mohammed Daoudi. Magnifying subtle facial motions for effective 4d expression recognition. *IEEE Transactions on Affective Computing*, 2017.
- [24] Alex Krizhevsky, Ilya Sutskever, and Geoffrey E Hinton. Imagenet classification with deep convolutional neural networks. In *Advances in neural information processing systems*, pages 1097–1105, 2012.
- [25] Olga Russakovsky, Jia Deng, Hao Su, Jonathan Krause, Sanjeev Satheesh, Sean Ma, Zhiheng Huang, Andrej Karpathy, Aditya Khosla, Michael Bernstein, et al. Imagenet large scale visual recognition challenge. *International journal of computer vision*, 115(3):211–252, 2015.
- [26] Christian Szegedy, Vincent Vanhoucke, Sergey Ioffe, Jon Shlens, and Zbigniew Wojna. Rethinking the inception architecture for computer vision. In *Proceedings of the IEEE conference on computer vision and pattern recognition*, pages 2818–2826, 2016.
- [27] Kaiming He, Xiangyu Zhang, Shaoqing Ren, and Jian Sun. Deep residual learning for image recognition. In *Proceedings of the IEEE conference on computer vision and pattern recognition*, pages 770–778, 2016.